(Author responses are in blue. In the tracked changes version deleted sequences are marked red. New text is marked in blue.) General Comment: We want to thank the three reviewers for the detailed reviews with many useful ideas and suggestions which, we think, have significantly increased the quality of the manuscript. We have rewritten a substantial portion of the manuscript. We restructured the outline of the manuscript. Section 2, formerly named "ALOMAR RMR Lidar" is now called "Instrument and Method" with subsections 2.1 "Processing of the raw data", 2.2 "Calculation of backscatter ratios" and 2.3 "Identification of the stratospheric aerosol layer". Section 3, formerly named "Methodology" is now named "Calculating the backscatter ratio under daytime conditions". Section 4 contains the results of the paper. A "Summary and Conclusion" can be found in section 5. The nomenclature for the calculation of the backscatter ratio and the color ratio was changed. Therefore, sections 2.2 and 3 have been completely rewritten. The figures have been updated to account for the new symbols.

In the paper, "Year-round stratospheric aerosol backscatter ratios calculated from lidar measurements above Northern Norway", the authors present a multiyear stratospheric sulfate aerosol (SSA) dataset from lidar observations at the ALOMAR research station. This paper provides valuable insight into lidar-measured SSA over the Arctic, and the study is appropriate for AMT, however I have a few major concerns with the paper in its current form. These include the overall writing quality of the manuscript and lack of important details of the study. Thus, I recommend a major revision. The authors should address the major and minor comments outlined below for the revised manuscript.

1. Writing quality of manuscript: Many grammatical errors and misspellings are found throughout the text, and acronyms need to be defined. The paper should be thoroughly proofread.

The paper has been reworked completely to improve the writing quality.

2.Lack of study details: There are several instances in the manuscript that I believe need additional information, as follows:

a. Page 4, Lines 7-10: Please add more description of ECMWF (e.g., spatial resolution). Why ECMWF? Are there other options? What are the uncertainties associated with the parameters from ECMWF?

   The section has been rewritten. We have selected the ECMWF model as it provides density and ozone data with a time resolution of 1 hour for the location of ALOMAR. We have briefly discussed the use of ozone values from another model in the manuscript (Page5, line 16).

   When you state "converted to a 5 min and 150 m grid", converted from what? Also, add more details on how the Rayleigh and ozone corrections are done.

   We interpolate the model data and the lidar data to a grid with a 5 minute time and 150 m vertical spacing. A special bullet point "Gridding of lidar data" has been added to section 2.1

b. Sensitivity studies: Please comment on the choices made, and any sensitivity studies completed for normalization altitudes (Page 5, Line 11), wavelengths for elastic/inelastic signals (Page 5, Lines 22-23), and lower limit of data availability (Page 7, Lines 13-14).

Normalization altitude: The approach was to use the highest possible altitude range as limited by the signal to noise ratio of the Raman backscattered light. This can be seen in Fig 2c: The Signal $S_3 87$ becomes exceedingly noisy at about 40 km, thus we used a range below. First, we used a range of 30-34 km (as suggested by previous publications) but the results showed, that the upper boundary of the aerosol layer was found above 30 km in many cases. Thus we have lifted the normalization altitude. We have improved section 2.2 accordingly.

Wavelengths: All elastic/inelastic wavelength combinations have been analyzed and lead to proper results. We focused on $R^1 064/387$ because of lowest effects due to Ozone extinction and highest backscatter ratios. This is now discussed in the revised manuscript.

Lower limit of data availability: We have improved the section 4 accordingly.

c. Equation 1 (Page 3): Where is this from (reference), or how was it determined?

The equation has been corrected. We have added a reference in the manuscript (Kovalev et al, 2004, "'Elastic Lidar: Theory, Practice, and Analysis Methods"', Page 138).

d. Page 6 (Section 4): Please add more discussion/explanation for this section, and the importance/purpose of each figure (Figures 4 through 7). For example, why are you showing $R355/387$ for Figure 5 instead of R at other wavelengths?

The section has been reworked completely. The correction is presented in more detail.

Also, please state why a correction is needed for $CR1064/355$.

The correction is now explained in detail in the discussion of equations 8 to 11.

e. Page 7 (Figures 9 and 10): Explain how these figures were created (e.g., averaging), as was included in the figure captions.

We have updated the manuscript accordingly: We first calculated hourly averaged backscatter ratios smoothed in altitude with a running mean of 1.1 km. Then we calculated the average for the two telescopes. Finally the mean of the hourly profiles is calculated for each month.

3. Conclusions: I believe this entire section needs to be re-worked. Please address the following:

a. Re-define all acronyms.

b. I recommend not referencing figures in this section.

c. Please do not state results that have not been already discussed earlier in the paper. For example, the uncertainties stated in Line 10 of Page 8. This belongs in the Results section.

d. As mentioned above there are grammatical errors in this section.

e. The narrative does not flow well (including ending with a lone sentence), so I recommend re-writing the entire section.

f. I suggest including bullets or something similar to summarize the main findings of the study.

The section has been reworked completely to account for all the comments.

Minor comments: 1. Page 1, Lines 1-12: Please add a few sentences to the abstract describing the primary results of the study.

Done. Abstract has been reworked

2. Page 1, Line 5: Define ALOMAR.

Done

3. Page 1, Line 15: Define SSA. All acronyms should be defined at their first use in the paper.

Done

4. Introduction section: State the location and dates of the study.

Done

5. Page 2, Lines 31-33: lidar measurements of what? R and CR? Explain the parameters of interest. Also, add more motivation as to why this study is important. What is being accomplished/what is the general purpose of this paper?

6. Page 3, Line 5: Add the elevation of the ALOMAR station.

Done

7. Pages 3 and 4 (Section 2): I suggest not using dashes when listing the processing steps. Bullets may work better.

Done

8. Page 4, Line 14: How was this relative uncertainty computed? Please add an explanation to the text.

This section was rephrased to provide the explanation in the manuscript.

9. Page 6, Lines 1-2: The layers are also not associated with PSCs because of the PSC screening metrics described on Page 5, correct?

Correct. We added this information now in the manuscript.

10. Page 7, Line 20: Rephrase "The first picture".

Done

11. Page 7, Line 31: Significantly lower altitudes? Are you comparing 12-18 km to 12-22 km? If so, this sentence does not make sense. This paragraph is confusing, so I recommend revising it.

The paragraph was split, because 2 different effects are discussed. The altitude ranges where not meant to be discussed together. This was made clearer.

12. Page 8, Lines 1-4: How do these findings compare with other studies?

We have included a brief comparison to previous studies in section 4.

13. Figure 2: Add labels, like a-d, to the plots, and refer to them in the caption. How was the altitude range of the stratospheric aerosol layer determined? Also, as a general comment, mention whether the altitudes are referenced to above ground level (AGL) or above mean sea level (AMSL). This should be stated in the text of the paper as well.

We added labels and used them in caption. The altitude range of the aerosol layer in this figure is 15 to 34 km and indicates the altitude range between a high tropopause and the lower boundary of the normalization altitude. All altitudes are referenced to AMSL. This is now stated in the revised manuscript.

14. Figure 4: For the x-axis, I suggest not using a slash symbol (/) here, as this could be confusing. Maybe use "or" instead. Also, the colored shaded areas representing the measurement uncertainties are very difficult to see.

We now use "or" as suggested. The uncertainties are pretty small and therefore hard to see. However they become visible above about 28 km.

15. Figure 5: Please mention in the caption what the shaded area in blue and black vertical line at R355/387 = 1 represent.

The figure has been reworked to make the discussion clearer. We have changed the line color of the black vertical line to gray as this line is just drawn for reference.

16. Figure 8 caption: I suggest re-wording "Time of available data".

Changed to "'Available data in hours"'.

17. Figures 1-10: I suggest making the text larger for both the axes and color bars.

Done. All figures have been reworked.

(Author responses are in blue. In the tracked changes version deleted sequences are marked red. New text is marked in blue.) General Comment: We want to thank the three reviewers for the detailed reviews with many useful ideas and suggestions which, we think, have significantly increased the quality of the manuscript. We have rewritten a substantial portion of the manuscript. We restructured the outline of the manuscript. Section 2, formerly named "ALOMAR RMR Lidar" is now called "Instrument and Method" with subsections 2.1 "Processing of the raw data", 2.2 "Calculation of backscatter ratios" and 2.3 "Identification of the stratospheric aerosol layer". Section 3, formerly named "Methodology" is now named "Calculating the backscatter ratio under daytime conditions". Section 4 contains the results of the paper. A "Summary and Conclusion" can be found in section 5. The nomenclature for the calculation of the backscatter ratio and the color ratio was changed. Therefore, sections 2.2 and 3 have been completely rewritten. The figures have been updated to account for the new symbols.

This paper presents the analysis of stratospheric aerosols observations using the state of the art Rayleigh-Mie-Raman multiple wavelength lidar at ALOMAR. The strato- spheric aerosol layer is observed at 1064 nm with unprecedented high resolution. The topic of the paper is well suitable for publication in AMT. However the description of the data processing and the results should be improved and I recommend a major revision as detailed below.

Equation (1) page 3 for the dead time correction does not seem correct. The correct formulation is: N=Ncount/(1-tau Ncount)

Corrected

Page 6, lines 10-11, how equation 3 could be applied if the inelastic signal is not present?

We have used the inelastic signal as measured during the night. This was made clearer in section 2.3.

Page 6, lines 15-21, the justification for a linear correction with altitude of the R355/387 is not given. It may hide some instrumental problems in the lidar. This point should be discussed in more details.

A new paragraph was added to cover this comment in section 3: "First of all we have not identified an instrumental problem that leads to this linear decrease with altitude; for example an incomplete overlap function would affect both signals S355 and S387 in the same way. Furthermore Ozone extinction can be excluded as potential source of error as it has virtually no impact on these signals."

Also I wonder why the ratios R532/387 and R532/355 on Figure 4 fall below 1 in the lower altitude range. Is it a problem of detector saturation?

An explanation for this issue is now given in the manuscript: "'$R^5 32_3 87$ is affected by ozone extinction. By definition a backscatter ratio should not be smaller than 1. This indicates that the true ozone extinction may be different from that used for processing the data since the signal at $\lambda = 532$ nm is stronger affected by ozone extinction than the signal at $\lambda = 355$ nm. Due to the normalization of the backscatter ratio to 1 in the aerosol free altitude z_F an under-estimation of ozone extinction reduces the backscatter ratio and may result in $R < 1$. A similar effect arises due to a wavelength dependent extinction of the aerosol layer. Here R is reduced at lower altitudes if the wavelength of the elastic backscattered signal is more affected by aerosols than the Raman wavelength."'

Results section page 7 How the standard error of the monthly mean scattering ratio is computed? Is it from the statistical error on lidar signal at different wavelengths? Due to the limited number of available hours of measurements per month and the large variability of the Artcic stratosphere, especially during winter months, the monthly averaged value of the scattering ratio cannot be considered as fully representative of the monthly climatological value for this month.

The standard error of the monthly mean backscatter ratio is computed like follows: $\sigma_m(R) = \sigma/sqrt(n)$ with sigma being the standard deviation of the backscatter ratio for each month and n being the measurement time in hours for each month. This information is now included in the revised manuscript.

Page 7, lines 27-29, the increase of aerosol loading in the lower stratosphere in August- September due to smoke from the Canadian fires merits to be discussed in more details than just put in the mean seasonal cycle.

A reference to a detailed discussion of the event is now given in the revised version. We mention the wildfires just shortly as a confirmation for the reasonable results of the aerosol retrieval.

(Author responses are in blue. In the tracked changes version deleted sequences are marked red. New text is marked in blue.) General Comment: We want to thank the three reviewers for the detailed reviews with many useful ideas and suggestions which, we think, have significantly increased the quality of the manuscript. We have rewritten a substantial portion of the manuscript. We restructured the outline of the manuscript. Section 2, formerly named "ALOMAR RMR Lidar" is now called "Instrument and Method" with subsections 2.1 "Processing of the raw data", 2.2 "Calculation of backscatter ratios" and 2.3 "Identification of the stratospheric aerosol layer". Section 3, formerly named "Methodology" is now named "Calculating the backscatter ratio under daytime conditions". Section 4 contains the results of the paper. A "Summary and Conclusion" can be found in section 5. The nomenclature for the calculation of the backscatter ratio and the color ratio was changed. Therefore, sections 2.2 and 3 have been completely rewritten. The figures have been updated to account for the new symbols.

The paper is appropriate for AMT, but not in a good shape. Major revisions are needed. The paper is much too long. Basic lidar stuff is unnecessarily presented in large detail. A compact version is needed.

Introduction: The importance of the SSA is presented in large detail! Why? One paragraph would be sufficient! On the other hand, one has to read the entire paper to get an idea: What is new here? What is the motivation to write this paper? Figures 9 and 10 tell the reader finally what the step forward is.

The manuscript was rewritten in large parts. We think that the novelty of the method and the motivation for the paper is now clear.

Please provide the motivation right in the beginning (second paragraph of the introduction): precise and compact. The shorter the introduction the better.

We now mention the motivation at the end of the introduction. We tried to shorten the introduction and also tried to take the other referees comment into account.

Maybe mention also that CALIOP observations are available to monitor SSA as well, but the disadvantage is. . ..

We did not include more discussion here as CALIOP does not provide stratospheric backscatter ratios at 1064 nm (Vernier et al., JGR, 2009). A detailed comparison of CALIOP and ground based lidar is given in Khaykin, ACP, 2017.

Section 2: . . .is much too long. One paragraph and good references would be fine. Section 2 could be even left out..., could be the introductory part of Section 3 (Method).

As described in the general comment, the section has been completely rearranged and also shortened.

There are many sentences that must be simply improved: The detection system is capable to detect wavelengths? Simply bad wording. . . The lidar detects backscatter signals at different wavelengths. There so many, many more examples throughout the paper. . .. , e.g., P5, L5:We use an inelastic counter for the denominator of Eq 2. . . unbelievable wording. So bad! So low quality of precise thinking! Did any of the co- authors (including the director . . .) read the manuscript?

The whole manuscript has been revised.

P5, L5: The reference is Raman, 1928! I could not believe what I read! Please provide a proper Raman LIDAR (!) reference here. The same for

Rayleigh, 1871, 1899. Please provide a proper Rayleigh lidar reference.

The section "Calculation of backscatter ratios" has been reworked completely.

Eq.(3), Eq(4): Please note! Quantities in equations are presented as ONE letter (a, b, c, T , p, that's why we use so often alpha, beta, gamma, ... and lambda, and then with index. . . if needed). So, please improve Eqs. 3 and 4 accordingly.

Done. The whole nomenclature for the derivation of the backscatter ratio was reworked.

P5, L29: . . .data is reduced to altitudes above the tropopause. . . another example of bad wording. . .

Rephrased

Section 4: I give up. . .! . . .. only a few remarks : purple drawn profile . . . or drawn as a red shade. . .. Please avoid 'drawn'!... In many cases, you can leave it simply out, some- times one may use: . . . is shown as purple curve, or given as red profile etc. . .

The section "Results" has been reworked completely.

So, this new procedure should be already briefly explained in the Intro section.

Done

Year-round stratospheric aerosol backscatter ratios calculated from lidar measurements above Northern Norway

Arvid Langenbach[1], Gerd Baumgarten[1], Jens Fiedler[1], Franz-Josef Lübken[1], Christian von Savigny[2], and Jacob Zalach[2]

[1]Leibniz Institut für Atmosphärenphysik an der Universität Rostock, Schlossstraße 6, 18225 Kühlungsborn
[2]Universität Greifswald, Felix-Hausdorff-Str. 6, 17489 Greifswald

Correspondence to: Arvid Langenbach (langenbach@iap-kborn.de)

Abstract.

~~In this work, the processing of a year-round~~ We present a new method for calculating backscatter ratios of the stratospheric sulphate aerosol (SSA) ~~dataset~~ layer from day- and nighttime lidar measurements~~is presented. The SSA layer is of fundamental importance for the radiative balance of the atmosphere. The layer is found~~ . Using this new method we show a first year-round dataset of stratospheric aerosol backscatter ratios at high latitudes. The SSA layer is located at altitudes between the tropopause and about 30 km. It is of fundamental importance for the radiative balance of the atmosphere. We use a ~~state of the art Doppler~~ state-of-the-art Rayleigh-Mie-Raman lidar at the ~~ALOMAR research~~ Arctic Lidar Observatory for Middle Atmosphere Research (ALOMAR) station located in Northern Norway (69° N, 16° E~~) to observe the aerosol layer and derive microphysical properties. The lidar allows the investigation of SSA from small spatial and temporal scales to decadal variations. The aerosol backscatter ratio is derived by using a multi-wavelength approach and different scattering processes. Here we~~ , 380 m a.s.l.). For nighttime measurements the aerosol backscatter ratios are derived using elastic and inelastic backscatter of the emitted laser wavelengths 355, 532 and 1064 nm. The set-up of the lidar allows to perform measurements with a resolution of about 5 minutes in time and 150 m in altitude with high quality, allowing to identify multiple sub-layers in the stratospheric aerosol layer of less than 1 km vertical thickness.

We introduce a method ~~for the extension of~~ to extend the dataset throughout the summer ~~where measurements have~~ when measurements need to be performed under permanent daytime conditions. ~~We calculate~~ For that purpose we approximate the backscatter ratios from color ratios of elastic ~~scattered light at the wavelengths 355, 532 and 1064 . These color ratios are corrected using an~~ scattering and apply a correction function. We calculate the correction function using the average backscatter ratio profile at 355 nm from about 1700 hours of nighttime measurements from the years 2000 to 2018. ~~Thereby, we are able to extend the dataset from 2883 of nighttime data to 7273 of total data time between 2000 and 2018.~~ Using the new method we finally present a year-round dataset based on about 4100 hours of measurements during the years 2014 to 2017.

1 Introduction

The ~~role of SSA~~ importance of stratospheric sulphate aerosol (SSA) for the radiative balance and the ozone chemistry of the atmosphere is widely accepted. Long-term observations of the stratospheric aerosol layer are crucial for the analysis of global atmospheric temperature and ozone layer variability (Tho, 2006; Solomon et al., 2011). First in situ measurements of SSA have been performed by Christian Junge and ~~coworkers~~ co-workers (Junge and Manson, 1961). They found a distinct layer between 15 and 25 km altitude with a peak at 20 km (Junge et al., 1961a, b). The stratospheric aerosol layer is therefore often referred to as ~~"~~Junge-layer~~"~~. Remote sensing of the aerosol layer by lidar was started by Bartusek and Gambling (1971). Global satellite observations of SSA began in the late 1970s ~~(reviewed by Tho (2006) and Kremser et al. (2016)).~~

(e.g. Tho, 2006; Kremser et al., 2016) . The upper boundary of the SSA layer is determined by the evaporation of the aerosol particles due to rising temperatures in the stratosphere as well as sedimentation (Hofmann et al., 1985). The tropopause is ~~generally known as~~ the base of the aerosol layer since the upper tropospheric aerosol ~~levels~~ loads are often much lower than in the stratosphere (Kremser et al., 2016).

Understanding ~~SSA~~ the formation and life-cycle ~~in the stratosphere~~ of SSA are impossible without understanding the processes controlling sulfur in the stratosphere. Stratospheric sulfur can be found in a broad variety of ~~gaseous~~ molecules, such as carbon disulfide (CS_2), sulfur dioxide (SO_2), carbonyl sulfide (OCS) and sulfuric acid (H_2SO_4) (English et al., 2011). ~~The composition of SSA is dominated by about~~ SSA typically consist of 75 % sulfuric acid/water ($H_2SO_4-H_2O$) solution droplets (Tho, 2006). In volcanically ~~quiescient~~ quiescent periods, the main source for these droplets are CS_2 and OCS~~. These compounds~~ , which are emitted at the Earth's surface and lifted into the stratosphere by deep convection and the Brewer-Dobson circulation (Khaykin et al., 2017). They then react in multiple steps via SO_2 into sulfuric acid (Kremser et al., 2016). Stratospheric aerosols are primarily washed out by sedimentation and through the quasi-isentropic transport of air masses in tropopause folds (Tho, 2006).

Moreover, the ~~stratospheric sulphate aerosol~~ SSA variability is dominated by major volcanic eruptions injecting sulfur directly into the stratosphere. These episodic but powerful eruptions can overlay the permanent stratospheric aerosol layer (referred to as ~~"background"~~ 'background' aerosol) for years and ~~can~~ have a global cooling effect on the surface in the order of a few tenths of a degree Celsius (Robock and Mao, 1995). ~~That~~ The fact that aerosols from large volcanic eruptions ~~can~~ have global effects was first determined by worldwide observations of optical phenomena following the eruption of ~~Krakatau~~ Krakatoa in 1883 (Symons, 1888). After the Mount Pinatubo eruption in 1991 the stratospheric sulfur burden was increased by a factor of 60 above background levels and remained ~~heightened~~ elevated by a factor of 10 well into 1993 (McCormick et al., 1995).

The long-term development of SSA has been discussed in various studies ~~(reviewed by Kremser et al. (2016)). Observations covering the timespan~~ (Kremser et al., 2016) . Ignoring periods with volcanically enhanced SSA, observations covering the time span between 1970 and 2004 did not show significant changes in the background aerosol (Deshler et al., 2006). Newer ~~works~~ studies show rising levels of SSA since 2002 (Hofmann et al., 2009; Vernier et al., 2011; Trickl et al., 2013; von Savigny et al., 2015). The reason for this increase is being debated. Originally the rise of the aerosol levels was connected

to a fast increase in Asian sulfur emissions ~~, lifted into the stratosphere though deep convection in the Asian monsoon (Hofmann et al., 2009) . Also, more~~ (Hofmann et al., 2009) . More recent studies show an increase in ~~nonvolcanic aerosol compounds~~ non volcanic aerosol inside of the Asian Tropopause Aerosol Layer~~(ATAL)~~. This layer occurs during the northern summer above the Asian monsoon (Vernier et al., 2015; Yu et al., 2015). Vernier et al. (2011) showed with the help of global satellite observations ~~,~~ that weaker eruptions also ~~inflect~~ influence the stratospheric aerosol layer. ~~Several studies have shown, that although these~~ These moderate eruptions are much less powerful than El Chichón or Pinatubo and the effect on stratospheric aerosol levels are much smaller~~,~~. However, several studies have shown that they have an impact on global surface temperatures ~~(Solomon et al., 2011; Fyfe et al., 2013; Santer et al., 2014, 2015; Andersson et al., 2015) .~~ nevertheless (Solomon et al., 2011; Fyfe et al., 2013; Santer et al., 2014, 2015; Andersson et al., 2015) .

Accurate long-term measurements are essential to quantify background, volcanic and anthropogenic changes in the stratospheric aerosol layer.

~~While balloon- or rocket-borne instruments deliver information only sporadically and satellites have to average data over a large area, lidar measurements are capable of ensuring the continuity and coherence~~ While there have been several reports on seasonal and decadal scale ground based lidar measurements of the aerosol layer at middle latitudes (Trickl et al., 2013; Khaykin et al., 2017 are no year-round or multi year measurements of the stratospheric aerosol ~~record at a certain location~~layer at high latitudes.

The ~~structure of the paper is as follows, in section 2 the lidar, as well as the data processing steps, are described. Following, in section ?? the calculation of the aerosol backscatter ratio R and the color ratio CR is explained. We then move on to section 3 , where the methodology of~~ main goal of this study is to present a year-round stratospheric aerosol record at polar latitudes for the first time, applying elastic laser scattering at three different wavelengths including measurements under full daylight conditions. This study introduces a method to approximate backscatter ratios of the stratospheric aerosol based on measurements of color ratios including a quantification of uncertainties. For this we use elastic and inelastic scattering measured during nighttime in the years 2000 to 2018. To show the performance of the new method we focus on a year-round dataset accumulated between 2014 to 2017. In section 2 the instrumental set-up and the data processing is described. Section 3 summarizes the extension of the dataset ~~throughout the summer is discussed, followed by the results in section 4 and conclusions~~using measurements performed during permanent daylight in summer. In section 4 we apply this new method to the years 2014 to 2017 and present a year-round climatology of SSA backscatter ratios.

2 ~~ALOMAR RMR lidar~~Instrument and Method

The Rayleigh-Mie-Raman lidar ~~is one of the core instruments~~ used in this study is installed at the Arctic Lidar Observatory for Middle Atmosphere Research (ALOMAR) ~~on the island of Andøya~~ in Northern Norway (69.3° N, 16.0° E, 380 m a.s.l.). The ~~main task is to perform studies of~~ lidar is employed for investigating the Arctic middle atmosphere ~~over altitudes of about~~ in the 15 to 90 km altitude range (von Zahn et al., 2000). The instrument is optimized to measure ~~simultaneously~~ atmospheric temperatures, winds and aerosols (Fiedler et al., 2008; Baumgarten, 2010). The ~~RMR lidar consists of two independent~~ lidar uses two power lasers and two receiving telescopes~~and is therefore also referred to as a twin-lidar system. The emitting wavelengths~~

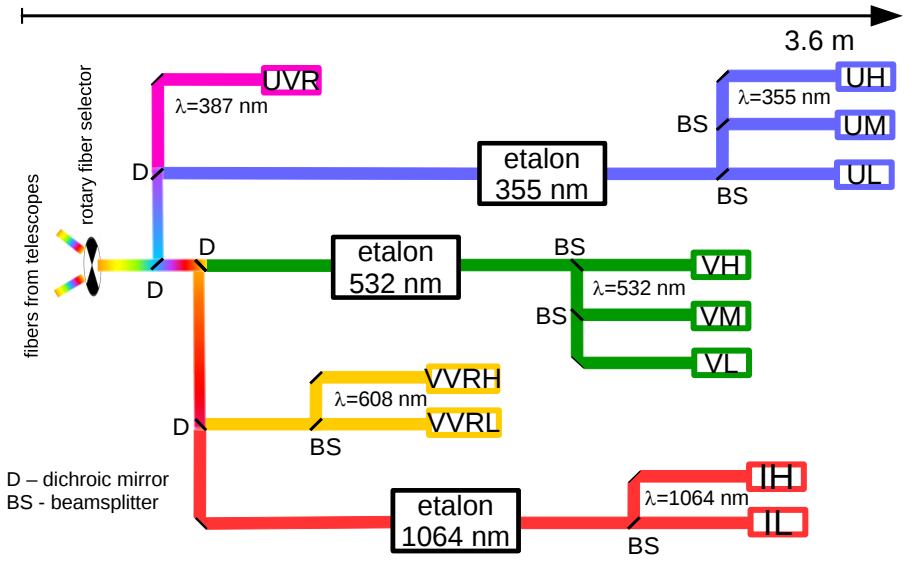

Figure 1. Simplified overview of the detection system of the lidar. The light collected by the two telescopes enters the detection system through a fiber selector (left) that is synchronized to the lasers. It is then separated according to wavelength with dichroic mirrors (D) and according to intensity by beamsplitters (BS). In daylight conditions, the light is guided through etalons to suppress solar background. At the end of each detection branch, the photons are converted to electrical pulses using avalanche photo diodes and photomultiplier tubes. The names of these detectors are formed as follows: first letter: spectral range (U-ultraviolet, V-visible, I-infrared), last letter: sensitivity (L-low, M-middle, H-high). Middle letters "VR" indicate vibrational Raman scattered light.

. Each of the two Nd:YAG power lasers ~~are 1064, 532 and 355 . They produce~~ generates 30 pulses per second with a ~~duration of about 10~~ pulse energy of 165, 500, and 465 mJ at the wavelengths of 1064, 532, 355 nm, respectively. The telescopes ~~are independently~~ have a diameter of 1.8 m and are tiltable from zenith pointing ~~up~~ to 30° off-zenith ~~. One telescope can be tilted to the north-west quadrant (NWT[1]) and the other one to the south-east quadrant (SET[1]), to perform measurements~~ to perform wind measurements and observations in a common volume with sounding rockets (Baumgarten et al., 2002). ~~To maximize the overlap of the field of view of the telescopes with the laser beams, the beams are emitted into the atmosphere coaxially with the line of sight of the telescopes.~~

The light collected by the telescopes is ~~alternatingly coupled~~ coupled alternatingly into the detection system ~~by a segmented mirror rotating with 30 . Fig~~synchronized to the alternatingly firing lasers. Fig. 1 shows a schematic overview of the detection system, limited to the channels used in this study. The light is separated ~~into different wavelengths using dichroic mirrors~~according to wavelength using dichroic beam splitters. The detection system is capable of detecting backscattered light at seven wavelengths during night-time (elastic: 355, 532, 1064 nm; inelastic: 387, 529, 530, 608 nm)~~and~~ . During daytime

[1] ~~north west telescope~~
[1] ~~south east telescope~~

the system detects backscattered light at three elastic wavelengths ~~during daytime~~ (355, 532, 1064 nm) using ~~etalon systems to oppress~~ additional Fabry-Pérot etalon based filters to reduce the solar background ~~(for details see von Zahn et al. (2000)). The three elastic wavelengths~~ (von Zahn et al., 2000) . The lidar measurements have been used before for calculating ~~properties of ice particles at the mesopause (e.g. von Cossart et al. (1999); Baumgarten et al. (2008))~~particle properties in the mesosphere and the upper stratosphere (e.g. von Cossart et al., 1999; Baumgarten et al., 2008; Gerding et al., 2003) . For the study of aerosols in the stratosphere, the channels were extended with intensity cascaded detectors to allow for simultaneous measurements from the troposphere to the mesosphere. ~~Then, the generated signals are processed by a complex data acquisition and control system. We calculate the measurement uncertainty from the actual count of photons assuming a Poisson distribution. This uncertainty of the raw counts is then propagated through the following processing steps: Deadtime correction - After~~ The backscatter signal is recorded with a time and range resolution of 30 seconds and 50 m, respectively.

2.1 Processing of the raw data

Before we start the actual aerosol retrieval we perform the following steps:

- Dead time correction

  Once a photon is ~~counted by a detector~~detected, a minimum time span has to ~~go by~~ pass before another photon can be ~~counted. This deadtime~~ detected. This dead time τ is about 20 to 50 ns for the ~~used detectors~~ detectors used in this study. The corrected number of counted photons N is calculated from the ~~deadtime~~ dead time and the count rate ~~N_{count}:~~ N_c (Kovalev and Eichinger, 2004) :

  $$N = \frac{1}{1 - \tau \cdot N_{count}} \frac{N_c}{1 - \tau \cdot N_c} \quad (1)$$

  ~~Background subtraction -~~

- Background subtraction

  The telescopes also collect light from scattered solar photons, stars or airglow. ~~Therefore the signal from far~~ The mean signal from above 100 km ~~, where no laser light is been received,~~ represents this background signal since backscattered laser light from these altitudes is negligible. This mean is subtracted from the ~~signal in all altitudes . Correction for Rayleigh-Extinction - The~~ signals at lower altitudes.

- Gridding of lidar data:

  The raw data is averaged in time for 5 minutes and in altitude to bins of 150 m taking into account the different pointing angles of the telescopes. All altitudes in this work are referenced to the mean sea level.

- Correction for extinction by Rayleigh scattering

  The intensity of the outgoing laser beam decreases slightly with altitude since a small fraction of the laser light is ~~continuously scattered out of the beam~~scattered by air molecules and aerosols. This also ~~happens for~~ reduces the scattered, downward propagating light. The magnitude of this effect depends on the wavelength and the density of the atmo-

sphere (Penndorf, 1957). ~~Correction for Ozone-Extinction - Amongst other wavelengths, stratospheric Ozone absorbs light between 400 and 900 (?) . The wavelengths affected most strongly (by~~ We use air densities from a numerical weather prediction model (see below).

- Correction for extinction by ozone

  Some part of the laser light is absorbed by O_3, in particular in the Chappuis bands ~~) are~~ affecting the laser wavelengths 532 and 608 ~~nm. The~~ nm. This effect is corrected using the O_3 absorption cross sections ~~are taken from Gorshelev et al. (2014)~~ from Gorshelev et al. (2014) and the O_3 mixing ratios and air density from a climatological model (see below).

- Combination of intensity cascaded detectors

  We combine the signals of intensity cascaded detector groups by normalizing the lower intensity signal to the higher intensity signal in an altitude range where both detectors provide a sufficient signal S with a relative uncertainty of better than $\Delta S/S < 0.1$. ~~The correction for both ,~~

The measurement uncertainty ΔS is calculated from the initial count of photons assuming a Poisson distribution. This uncertainty of the raw counts is then propagated through the processing steps listed above.

We calculate the Rayleigh- and ozone-extinction ~~, is done using~~ using densities and ozone mixing ratios provided by the European Centre for Medium-Range Weather Forecasts (ECMWF)~~density and ozone mixing ratio data. We use~~ . The data from the Integrated Forecasting System ~~available per hour~~ of ECMWF is extracted for the location of ALOMAR ~~. Afterwards, the data is converted to a~~ on hourly basis. The model data is then interpolated to the lidar time and altitude bins (5 min and 150 m~~grid for each detector. The signals generated by a detector, processed and corrected are in the following referred to as a counter.~~

3 ~~Methodology~~

~~In order to retrieve vertical profiles of stratospheric aerosol, we first combine the counters with different sensitivity for each wavelength. This is done by normalizing the various energy cascaded levels and averaging the counters in altitude ranges, in which more than one counter is available. A relative measurement uncertainty of 0.1 is defining the uppermost altitude for each counter. The process is shown in Fig. 2. As a result, we get one continuous profile for each wavelength. A tabular overview of the different counters can be seen in table 1~~). We performed a sensitivity study using air densities from an empirical model (MSISE-00; Picone et al. (2002)) and a mean seasonal cycle for ozone (Rosenlof et al., 2015) . It turned out that this leads to unrealistic backscatter ratios as the actual ozone profile significantly deviates from the climatological mean, especially in winter (see discussion of ozone extinction in section 3).

~~The retrieval is based on the Fernald-Klett inversion method (Fernald, 1984; Klett, 1985) . The backscatter ratio R is derived as the ratio of the sum of aerosol and molecular backscattering to molecular backscattering:~~

$$R = \frac{\beta_{aero} + \beta_{mol}}{\beta_{mol}} = 1 + \frac{\beta_{aero}}{\beta_{mol}},$$

Table 1. ~~Overview~~ Labels of combined signals and individual detectors. The name indicates in the ~~ALOMAR RMR lidar counters used for this work~~first letter the spectral range (U-ultraviolet, V-visible, I-infrared), and with the last letter the sensitivity (L-low, M-middle, H-high). The letter pair "VR" indicates vibrational Raman scattered light. Indices represent the particular wavelength.

combined ~~counter~~ signal	~~counter on optical bench~~ detector	scattering process	daylight capability
S^{355}	UL_{355}	elastic (Rayleigh and Mie)	yes
	UM_{355}		
	UH_{355}		
S^{532}	VL_{532}	elastic (Rayleigh and Mie)	yes
	VM_{532}		
	VH_{532}		
S^{1064}	IL_{1064}	elastic (Rayleigh and Mie)	yes
	IH_{1064}		
S^{387}	UVR_{387}	inelastic (Raman)	no
S^{608}	$VVRL_{608}$	inelastic (Raman)	no
	$VVRH_{608}$		

~~where β_{aero} and β_{mol} are the aerosol and molecular backscatter coefficients~~

The different detector groups and their corresponding scattering mechanisms are summarized in table 1. An example for the signals of individual detectors and the combined signals S^{λ} is shown in Fig. 2. The data is averaged for 17 hours starting at 13 UT on January 27, ~~respectively. Inelastic scattering only occurs on molecules (?) , therefore we are able to use an inelastic counter signal for the denominator of equation 3. Elastic scattering on the other hand appears on both , aerosols and molecules (??) . Hence it is possible to use a elastic counter signal as the numerator of equation 3.~~ 2018. About 7 hours were performed under daytime conditions while 10 hours of the measurement were performed under nighttime conditions. The telescopes were pointing for about 1.5 hours to zenith and for the rest of the measurement 20° off zenith towards North and East. For plotting the data we have calculated the mean signals of the two telescopes. For the elastic scattered signals we observe a sudden increase in the signals below 30 km which is caused by tropospheric (below about 10 km) and polar stratospheric clouds (~15 to 25 km).

~~Due to the much lower scattering cross section for inelastic scattering, the signal for inelastic counters can be some orders of magnitude smaller . Thus the signals have to be normalised in an aerosol-free altitude range on order to eliminate an aerosol influence on the normalization. This~~

2.1 Calculation of backscatter ratios

The standard method to characterize the aerosol content in the atmosphere from lidar signals is to calculate the backscatter ratio R from the molecule and aerosol backscatter coefficients β_m and β_a, respectively (see, (Fernald, 1984; Klett, 1985; Ansmann et al., 1990, e

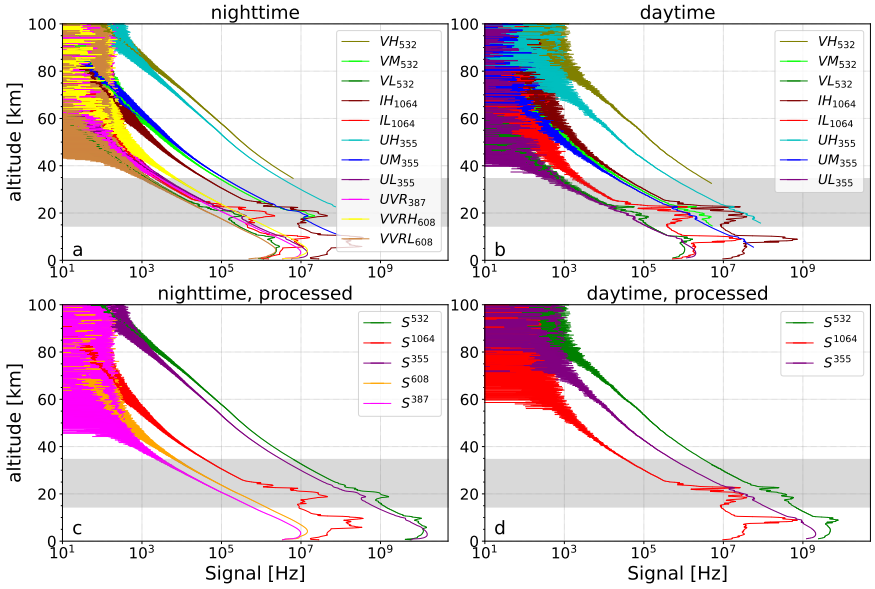

Figure 2. Time averaged altitude profiles of backscattered signals for a 17 hour long measurement starting at 13 UT on 27 January 2018. (a) and (b) show the count rates of individual detectors, (c) and (d) the resulting profiles after combining the signals of the different detector groups. (a) and (c) show about 10 hours of nighttime measurements and (b) and (d) about 7 hours of daytime measurements. The approximate altitude range of the stratospheric aerosol layer is shown in gray.

$$R = \frac{\beta_m + \beta_a}{\beta_m} \tag{2}$$

In our case the backscatter coefficients are proportional to the corrected signals S, shown in Fig. 2c. Let's for example consider scattering at $\lambda = 1064$ nm:

$$R^{1064} = \frac{S_m^{1064} + S_a^{1064}}{S_m^{1064}} = \frac{S^{1064}}{S_m^{1064}} \tag{3}$$

The challenge is to retrieve the signal scattered by molecules only (S_m^{1064}) since the signal received by the lidar (S^{1064}) contains both contributions from scattering on molecules and aerosols. For this we use the signal from Raman backscattering on N_2 at $\lambda = 387$ nm which contains molecular scattering only: S^{387}. Since Raman scattering is less efficient compared to Rayleigh and Mie scattering, S^{387} is much smaller compared to S_m^{1064} at any given altitude. However, using the correction and applying the processing steps in section 2.1 both signals are proportional to each other ($S^{387} \propto S_m^{1064}$) since they are both given by molecular scattering. We determine the proportionality constant F at an altitude ~~is considered to be above 30~~ z_F where no aerosols exist, hence S^{1064} equals S_m^{1064}, which is typically the case above 34 km~~(McCormick et al., 1984; Barnes and Hofmann, 1997; Khaykin et al., 20~~

~~We choose a normalization altitude~~ :

$$F_{387}^{1064} = \left\langle \frac{S^{1064}}{S^{387}} \right\rangle_{z=z_F} \tag{4}$$

This allows to derive S_m^{1064} at any given altitude:

$$S_m^{1064} = F_{387}^{1064} \cdot S^{387} \tag{5}$$

therefore Eq. 3 leads to:

$$R_{387}^{1064} = \frac{S^{1064}}{F_{387}^{1064} \cdot S^{387}} \tag{6}$$

This ratio is named R_{387}^{1064} to indicate the wavelength of the elastic backscattered signal ($\lambda = 1064$ nm) and the Raman wavelength ($\lambda = 387$ nm). We use the altitude range z_F from 34 to 38 km ~~because the inelastic signal is still strong enough and the total aerosol layer is found below. The normalization is performed in~~ to determine F_{387}^{1064} since an initial processing of the dataset showed that the aerosol layer sometimes reaches up to about 34 km. In addition to this rather high normalization altitude we use a two-step ~~iteration~~process to reduce the effect of an aerosol layer reaching partly up into the normalization altitude range. First, we calculate the mean signal ratio in the normalization range, then we limit the ~~signal ratio~~ data in the normalization range to those ~~altitudes within 1-sigma of the mean signal ratio . This procedure reduces the effect of an aerosol reaching up to the normalization layer~~where the signal ratio is within one standard deviation of the mean. More details on this are discussed in section 4. ~~Accordingly, equation 3 yields:~~

$$R = \left[\frac{Signal\ (inelastic)}{Signal\ (elastic)}\right]_{z(R=1)} \cdot \frac{Signal\ (elastic)}{Signal\ (inelastic)},$$

~~where $z(R=1)$ is the normalization altitude between 34 and 38 .~~

~~Furthermore the calculation of a color ratio CR is of importance. It describes a ratio of two elastic signals and is computed as follows:~~

$$CR = \left[\frac{Signal\ (elastic)(\lambda_0)}{Signal\ (elastic)(\lambda_1)}\right]_{z(R=1)} \cdot \frac{Signal\ (elastic)(\lambda_1)}{Signal\ (elastic)(\lambda_0)},$$

~~with λ_o~~ Additionally to $\lambda = 1064$ nm we also investigated the other two emitted wavelengths, namely $\lambda = 532$ nm and ~~λ_T being two elastic scattered lidar wavelengths.~~

~~There are multiple combinations of possible elastic and inelastic signals~~$\lambda = 355$ nm. In total we derive three backscatter ratios: R_{387}^{1064}, R_{387}^{532}, R_{387}^{355}, all as a function of altitude. Instead of the Raman signal at $\lambda = 387$ nm we have tentatively used another Raman signal, namely at a wavelength of $\lambda = 608$ nm. It turned out, however, that this is not practical since this signal is partly absorbed by ozone (see Sec. 3). In this work, we focus on ~~1064~~ R_{387}^{1064} i.e. $\lambda = 1064$ nm as the ~~elastic signal due to~~

the highest aerosol backscatter signal at this wavelength and 387 Rayleigh and Mie scattered signal and $\lambda = 387$ nm as the inelastic signalbecause it is only weak affected by ozone extinction ($R_{1064/387}$). Raman signal. This combination is superior to the others as ozone extinction does not affect these two wavelengths and the backscatter ratio is found to be largest at $\lambda = 1064$ nm.

Since only stratospheric aerosols are investigated in this study, the data is reduced to

2.2 Identification of the stratospheric aerosol layer

Only backscatter ratios from altitudes above the tropopause . This is done by using the ECMWF data for are analysed in order to limit the data to the stratospheric aerosol layer. We calculate the dynamical and the thermal tropopause for each time step. The backscatter ratio data is reduced to altitudes higher than the larger of these two tropopause values to exclude tropospheric airfrom ECMWF model data and select the higher value of the two as lower altitude limit for the backscatter ratio profiles.

Using this method also detects We also remove measurements that show the presence of polar stratospheric clouds (PSC) (see Peter (1997) for details). In winter, (Peter, 1997) . From December to February these clouds occur over ALOMAR frequently frequently at our location. The calculated backscatter ratio R of the PSCs is of PSCs is about one order of magnitude higher than for SSA and therefore overlying larger than that of the background aerosol . Thus, measurements with clear evidence of PSCs are removed from the dataset (e.g. Fig. 2), so we use a simple threshold of $R_{387}^{1064} > 2.0$ to exclude PSC from our dataset of stratospheric aerosols.

An example of a R measurement over 80 hours in February for a backscatter ratio R_{387}^{1064} of the stratospheric aerosol layer from 88 hours of measurement starting on February 18, 2018 is shown in Fig. 3. The result draws We observe a highly dynamic picture of the stratospheric aerosol layer consisting of multiple sub-layers. There are several layers thinner than one km of aerosol above 20 visible over remaining separated and partially moving in parallel over several days. It should be emphasized that these layers are not connected with PSCs since to PSCs for two reasons: (1) The maximum backscatter ratio is well below the PSC threshold of $R_{387}^{1064} = 2.0$ and (2) the temperatures at the time altitudes of the layers were above 210 K and therefore too high for PSC formation . The measurement only shows stratospheric background aerosol . With the described methodology an investigation of stratospheric aerosol above ALOMAR on unprecedented time scales becomes possibleabout 15 K above PSC formation temperature (Beyerle and Neuber, 1994) .

Fig. 3 shows the evolution of the stratospheric aerosol layer during night and day. As the signal S^{387} (needed to calculate R_{387}^{1064}) is not measured during daytime we have calculated the mean signal S^{387} during the night measurements (indicated in Fig. 3) and used this mean profile to calculate R_{387}^{1064}. Fig. 3 shows that this method of calculating the backscatter ratio during daytime (using a nearby nighttime measurement) results in a reasonable evolution of the backscatter ratio.

3 Dataset expansion to daylight Calculating the backscatter ratio under daytime conditions

The ALOMAR RMR lidar is situated at 69.3° N, i.e. north of the Polar circle, requiring day configuration all summer. The stratospheric aerosol retrieval uses an inelastic scattering counter which is available at night only (see table 1). At this latitude

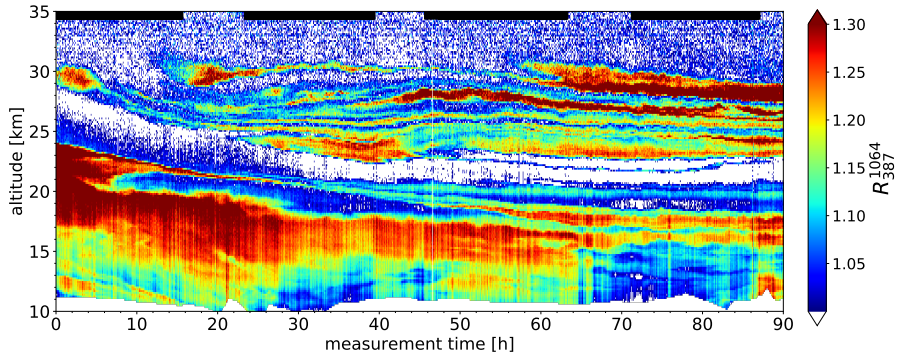

Figure 3. Stratospheric aerosol backscatter ratio (R_{387}^{1064}) for a measurement starting at 15:30 UT on 18 February 2018. The time resolution is 5 minutes and the altitude resolution is 150 m. Black bars at the top indicate nighttime configuration. At the bottom end of about 11 km the data at altitudes below the tropopause is masked (white).

the daytime configuration of the lidar is used from about mid May to mid August. As shown in the previous section the backscatter ratio can be calculated for daytime measurements using a nearby nighttime observation. Unfortunately this is not possible during the summer months due to the permanent daylight. In order to retrieve a solid year-round dataset, we use ~~a multi-color approach and correct a~~ the year-round available color ratio ~~CR of two elastic scattering counters~~C_{355}^{1064} with an empirical correction as a proxy for the backscatter ratio R_{387}^{1064}.

~~The starting point are the profiles depicted in Fig. 4. Shown are two backscatter ratios (green: $R_{1064/387}$, blue: $R_{355/387}$), which are calculated by using equation 6. This equation is also applicable if the inelastic signal is not available during the whole measurement run, i. e. if the daytime configuration was used partly during the run. Also shown is a color ratio (red: $CR_{1064/355}$) which~~ We define the 'color ratio' C, namely the ratio of signals received from two of the three wavelengths (1064 nm, 532 nm, 355 nm) normalized to the signal ratio at an altitude (z_F) where no aerosols exist. This is similar to the procedure for calculating the backscatter ratio in section 2.1 and yields, as an example, for 1064 nm and 355 nm:

$$C_{355}^{1064} = \frac{S^{1064}}{F_{355}^{1064} \cdot S^{355}} \tag{7}$$

It is worth noting that the definition of a color ratio used here is different from that used in von Cossart et al. (1999) and Baumgarten et al. (2008) .

Fig. 4 shows the mean backscatter ratio and color ratio profiles for a typical measurement in October 2015. The measurement lasted for 97 hours, thereof 46 hours with daytime configuration and 51 hours with nighttime configuration. Here, the backscatter ratio for the daytime part of the measurement is calculated by using ~~equation **??**. The blue $R_{355/387}$ profile shows an aerosol part in the 355 Signal which explains the difference between red ($CR_{1064/355}$)~~the mean signal S^{387} during nighttime observation as described in Sec. 2.2. Comparing R_{387}^{1064} and ~~blue ($R_{1064/387}$) profile. As mentioned before, the red $R_{1064/355}$ profile is available year-round due to the daylight capability of the elastic channels of the ALOMAR RMR lidar.~~

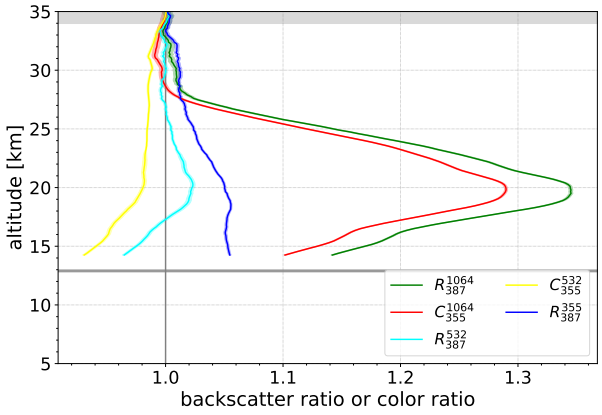

Figure 4. Backscatter ratio and color ratio profiles for a 97 hour long measurement starting at 07:45 UT on 10 October 2015. About 46 hours were measured with daytime configuration and 51 hours with nighttime configuration. The gray area at the top indicates part of the normalization altitude. Shaded areas around the lines indicate the measurement uncertainty. The gray line at 13 km indicates the tropopause.

C_{355}^{1064} we see that C_{355}^{1064} has nearly the same vertical structure but is about 5 % lower than R_{387}^{1064}. The difference between R_{387}^{1064} and C_{355}^{1064} is primarily due to the aerosol backscatter signal S_a^{355} included in the signal S^{355}. In other words, the color ratio C_{355}^{1064} is a proxy for R_{387}^{1064} that deviates by less than about 5 % from the true value of R_{387}^{1064} at the peak of the stratospheric aerosol layer. In the following we describe a method how to calculate the backscatter ratio at 1064 nm with respect to the molecular signal at 355 nm (R_{355}^{1064}):

$$R_{355}^{1064} = \frac{S^{1064}}{F_{355}^{1064} S_m^{355}} \tag{8}$$

This can be rewritten using the color ratio C_{355}^{1064} and the backscatter ratio R_{387}^{355}:

$$R_{355}^{1064} \approx \frac{S^{1064}}{F_{355}^{1064} F_{387}^{355} S^{387}} \tag{9}$$

$$\approx \frac{S^{1064}}{F_{355}^{1064} S^{355}} \cdot \frac{S^{355}}{F_{387}^{355} S^{387}} \tag{10}$$

$$\approx C_{355}^{1064} \cdot R_{387}^{355} \tag{11}$$

Since the backscatter ratio R_{387}^{355} is not available for daytime measurements we approximate the actual profile by a mean of all available measurements, to calculate an approximated backscatter ratio R_{355}^{1064}. Figure 5 shows the mean R_{387}^{355} profile for each of the 103 ~~suitable $R_{355/387}$ averaged profiles from measurements runs~~ measurements between 2000 and 2018 ~~,~~ which cover a total of 1789 ~~of measurement. In order to find these profiles the dataset has been filtered for measurement runs without PSCs and with~~ hours. These measurements were selected as they have a relative backscatter ratio ~~measurement uncertainty smaller~~ uncertainty of less than one percent ~~. The $R_{355/387}$ profiles~~ ($\Delta R_{387}^{355}/R_{387}^{355} < 0.01$).

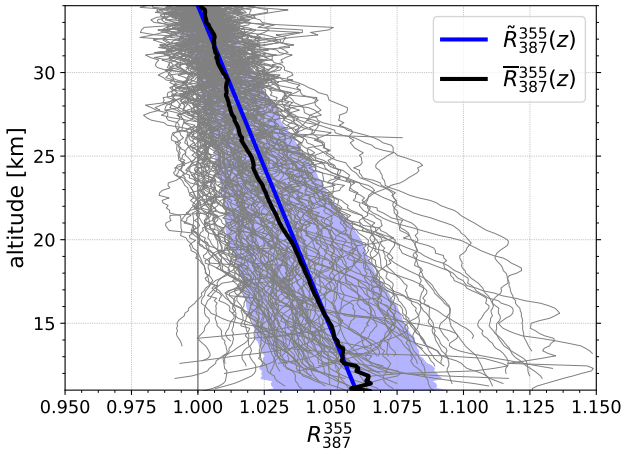

Figure 5. Backscatter ratios R^{355}_{387} from nighttime measurements in the period 2000 to 2018. Each gray line represents the mean of the measurement run. The total measurement time is 1789 hours. $\overline{R}^{355}_{387}(z)$ is the mean of all profiles and $\tilde{R}^{355}_{387}(z)$ a linear fit to $\overline{R}^{355}_{387}(z)$. The shaded area represents the standard deviation of the R^{355}_{387} profiles.

The profiles of R^{355}_{387} show a linear ~~behaviour towards $R \to 1$~~ decrease with altitude towards $R = 1$ at $z = 34$ km. ~~Therefore a~~ This behaviour is seen very well in the mean profile ($\tilde{R}_{355}(z)$~~)is calculated and fitted linearly with the altitude z:~~ $\overline{R}^{355}_{387}(z)$). We make use of this systematic altitude dependence by fitting a linear regression:

$$\tilde{R}_{355}{}^{355}_{387}(z) = \frac{z - 407.95\ \text{km}}{-374.16\ \text{km}} \tag{12}$$

~~The fit $\tilde{R}_{355}(z)$ is used to correct the $CR_{1064/355}$ profiles with the following equation:~~ Finally, we use the fit $\tilde{R}^{355}_{387}(z)$ to calculate the approximated backscatter ratio R^{1064}_{355}:

$$R_{1064/355}{}^{1064}_{355} = CR_{1064/355} C^{1064}_{355} \cdot \tilde{R}_{355}{}^{355}_{387}(z) \tag{13}$$

~~with $R_{1064/355}$ being the approximated backscatter ratio at 1064 . The result for the measurement is shown in Fig. 6. The new purple drawn profile $R_{1064/355}$ matches the true backscatter ratio (green: $R_{1064/387}$) well within measurement uncertainty. The higher total~~

Depending on altitude, the correction has a total effect on the backscatter ratio ranging from 5 % at 15 km to zero at 34 km. Fig. 6 shows the approximate backscatter ratio R^{1064}_{355} for the 97 hour long measurement in October 2015. The approximated backscatter ratio profile R^{1064}_{355} matches the backscatter ratio R^{1064}_{387} by better than 1 % which is well within the calculated uncertainty.

The uncertainty of the corrected profile is ~~caused by the measurement~~ dominated by the uncertainty of the ~~color ratio profile, the measurement uncertainties of the $\tilde{R}_{355}(z)$ linear fit and of the correction which is calculated as the mean difference~~

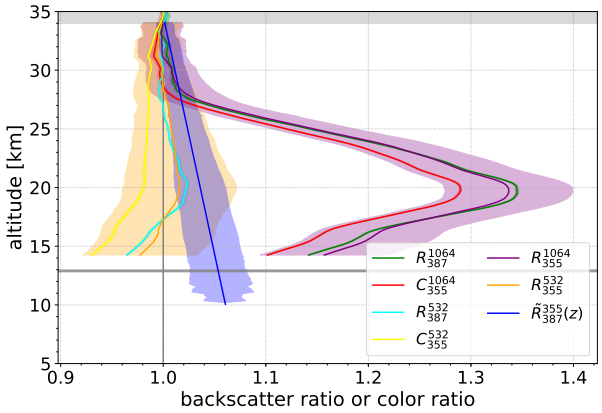

Figure 6. Backscatter ratio, color ratio, and approximate backscatter ratio profiles (R_{355}^{1064}, R_{355}^{532}) for a 97 hour measurement starting 07:45 UT on 10 October 2015, the same measurement as in Fig. 4. Colored shaded areas around the lines indicate the measurement uncertainty. Further explanations are given in Fig. 4.

~~between $R_{1064/387}$ and $R_{1064/355}$~~ linear fit $\tilde{R}_{387}^{355}(z)$. We have calculated the uncertainty of the fit as the standard deviation of the difference between R_{387}^{1064} and R_{355}^{1064} for each altitude. This difference is shown in Fig. 7 for each of the 103 ~~measurement runs where both these profiles are available between 2000 and 2018. The resulting standard deviation of this distribution is drawn as a red shade and defines the uncertainty for a single $R_{1064/355}$ profile as shown in the purple shaded area in Fig. 6.~~

~~The same correction can be done for the 532 branch of the lidar system. This is also shown in Fig. 4 and Fig 6. In this case,~~ measurements. It is symmetric over the whole altitude range and decreases with altitude. This behavior is as expected, as the effect of the correction tends to zero at 34 km and the R_{387}^{355} profiles for each measurement tend to $R = 1$ at 34 km.

In the same way an approximated backscatter ratio ~~$R_{532/355}$ (orange)~~ R_{355}^{532} is calculated from the corresponding color ratio ~~$CR_{532/355}$ (yellow) and the correction fit $\tilde{R}_{355}(z)$ to extend the $R_{355/387}$ backscatter ratio data (cyan)year-round. It is derived by the equation:~~

~~$R_{532/355} = CR_{532/355} \cdot \tilde{R}_{355}(z)$~~

C_{355}^{532} and the fit $\tilde{R}_{387}^{355}(z)$:

$$R_{355}^{532} = C_{355}^{532} \cdot \tilde{R}_{387}^{355}(z) \tag{14}$$

Both R_{387}^{1064} and C_{355}^{1064} are not affected by ozone extinction whereas R_{387}^{532} is affected by ozone extinction. We note that R_{387}^{532} is smaller than 1 in limited altitude ranges ($z = 15$ to 17 km). By definition a backscatter ratio should not be smaller than 1 (Eq. 3). This indicates that the true ozone extinction may be different from that used for processing the data since the signal at $\lambda = 532$ nm is stronger affected by ozone extinction than the signal at $\lambda = 355$ nm. Due to the normalization of the backscatter ratio to 1 in the aerosol free altitude z_F an under-estimation of ozone extinction reduces the backscatter ratio and may result

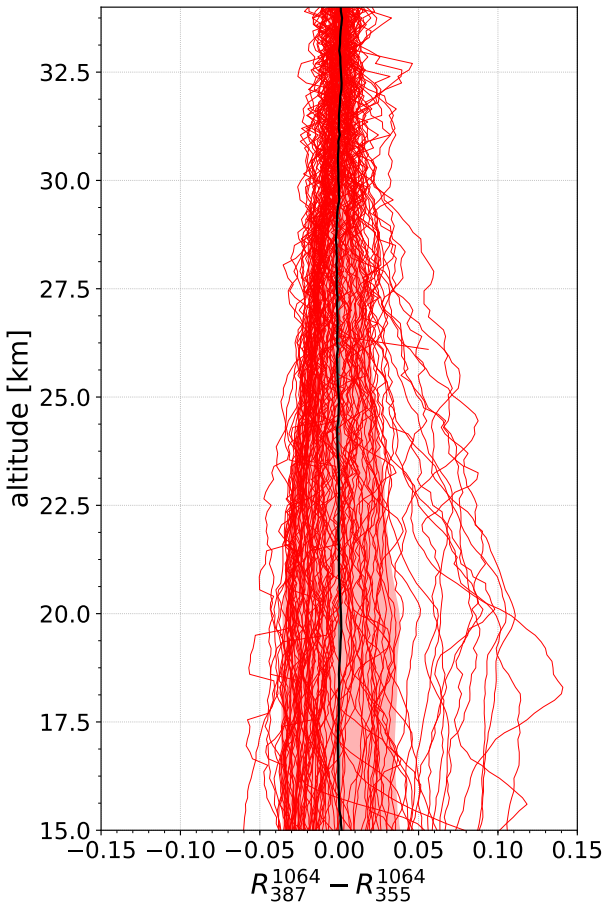

Figure 7. Difference of the backscatter ratio R^{1064}_{387} and the approximated backscatter ratio R^{1064}_{355} for 103 measurements between 2000 and 2018 where both ratios are available. The red shadowed area shows the standard deviation of the difference. The black line shows the mean difference.

in $R < 1$. A similar effect arises due to a wavelength dependent extinction of the aerosol layer. Here R is reduced at lower altitudes if the wavelength of the elastic backscattered signal is more affected by aerosols than the Raman wavelength (see Eq. 6).

~~In conclusion,~~ The quality of the approximated backscatter ratio R^{532}_{355} is also seen in Fig. 6 as it agrees now well to R^{532}_{387}. Notably R^{532}_{355} is larger than 1 in most altitudes (in contrast to C^{532}_{355}). We like to point out that approximated backscatter ratios underestimate the true backscatter ratios in cases of strong aerosol loads and overestimate the true backscatter ratios in cases of low aerosol loads since the correction function $\tilde{R}^{355}_{387}(z)$ was derived from measurements with a mean aerosol load.

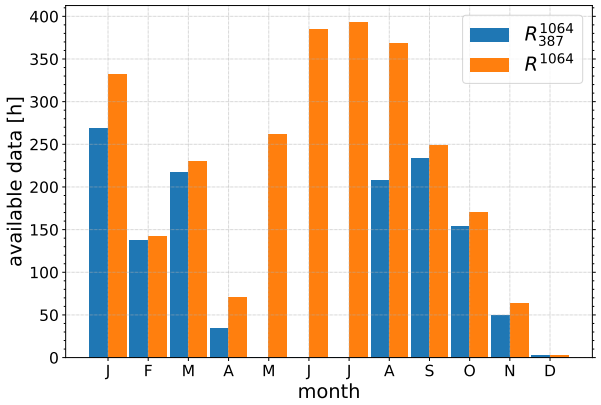

Figure 8. Available data in hours for each month for the years 2014 to 2017 for R_{387}^{1064} (blue) and R^{1064} (orange).

Although the backscatter ratios R_{355}^{1064} are only marginally affected by the actual shape of the correction function $\tilde{R}_{387}^{355}(z)$, it is worth discussing the linear decrease of $\tilde{R}_{387}^{355}$ with altitude. First of all, we have not identified an instrumental problem that leads to this linear decrease with altitude; for example an incomplete overlap function would affect both signals S^{355} and S^{387} in the same way. Furthermore ozone extinction can be excluded as a potential error source since it has virtually no impact on these signals.

Using this approach a new dataset ~~(R_{1064}) is composed, consisting of $R_{1064/387}$ profiles when available and $R_{1064/355}$ profiles when not~~R^{1064} is generated consisting of the exact backscatter ratio R_{387}^{1064} for nighttime configuration (or daytime configuration with nearby nighttime measurements) and the approximated backscatter ratios R_{355}^{1064} for the measurements in which only daytime configuration was applied (mostly summertime). The result is a ~~solid~~ complete year-round dataset of stratospheric aerosol backscatter ratio profiles.

4 Results

~~To show the performance of the new procedure of compiling a dataset of aerosol backscatter ratios R_{1064} we investigate the data from~~

We have applied the procedure described in Sec. 3 to the data of the years 2014 to 2017. ~~By choosing four recent years of lidar operations, we can well~~ During this period the lidar was operated for 4158 hours and allows to cover a typical seasonal cycle of the stratospheric aerosol. A total of 232 measurement runs were performed~~, collecting data we can use for the analysis~~. In 24 of those runs PSCs were detected and ~~thus~~ these runs were therefore excluded. The ~~208 remaining~~ remaining 208 runs represent 3646 hours of ~~measurement~~observations. Of these measurements ~~,~~ 2391 hours were performed ~~during daytime while~~ with daytime configuration and 1255 hours ~~were performed during nighttime~~ with nighttime configuration, respectively. Fig. 8 shows the ~~available monthly data time for the R_{1064} and $R_{1064/387}$ dataset between 2014 and 2017. For nearly every month~~

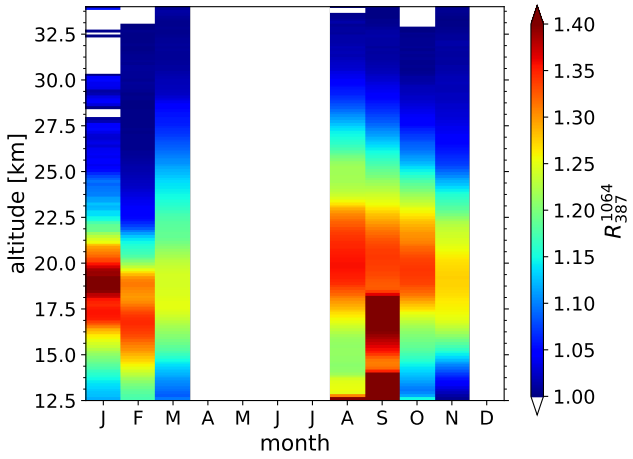

Figure 9. Monthly mean aerosol backscatter ratio R_{387}^{1064} from 79 measurement runs from 2014 to 2017. The dataset contains only nighttime measurements and includes a total of 1255 hours.

~~a gain in data time is reached by extending the $R_{1064/387}$ dataset to~~ hours of measurements for the combined dataset R^{1064} and the ~~R_{1064} dataset. The lone exception is~~ backscatter ratio R_{387}^{1064}. We see that the combined dataset includes the summer months where no measurements of R_{387}^{1064} are available. During the other months the R^{1064} dataset is larger as well, compared to the R_{387}^{1064} dataset.

We calculated the monthly mean backscatter ratios R_{387}^{1064} and R^{1064}, omitting the month of December ~~,~~where only 3 hours of ~~data are availablefor both datasets. We define a lower limit of data availability of 10 per month in order to obtain representative data. Furthermore, the standard error of the monthly mean backscatter ratio (σ_R) may not exceed 0.02. This value is not reached for any monthly average of the R_{1064} dataset, where σ_R is below 0.01 for every month. For the monthly average of the $R_{1064/387}$ dataset for April of 2014 to 2017 σ_R is about 0.025 due to a small dataset of only 35 with high variability. For all other months,~~ measurements are available. For this we first calculated hourly averaged backscatter ratios smoothed in altitude with a running mean of 1.1 km. Then we calculated the average for the two telescopes. Finally the mean of the hourly profiles is calculated for each month. The standard error of the mean is given by $\sigma_m = \sigma/\sqrt{n}$, where σ is the standard deviation and n is the ~~standard error is also below 0.01. These criteria lead to a lack of data in the $R_{1064/387}$ dataset for the months of April to July, and for December for both datasets~~number of measurement hours per month.

~~An example of the effect of the extension of the stratospheric aerosol dataset~~ The results for the nighttime backscatter ratio R_{387}^{1064} from 79 measurement runs is shown in Fig. 9~~and Fig. 10. Both these figures show a seasonal cycle of aerosol backscatter ratio over the time span 2014 to 2017. The first picture for the ratio $R_{1064/387}$ clearly lacks data between April and July, where no nighttime measurements were performed. The data illustrated in Fig. 9 was calculated from 79 measurement runs between~~

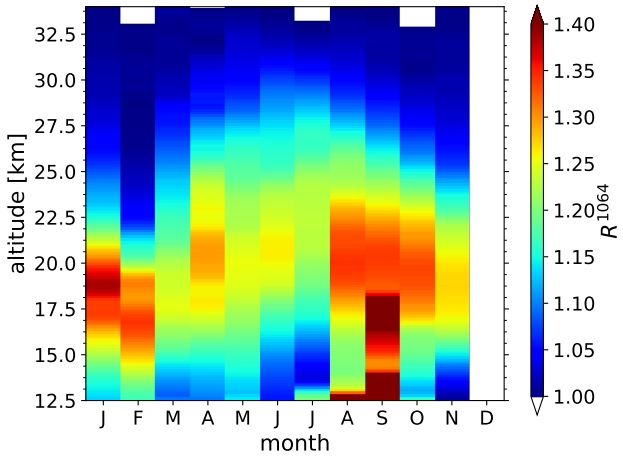

Figure 10. Monthly mean aerosol backscatter ratio R^{1064} from 208 measurement runs from 2014 to 2017. The dataset contains night and daytime measurements and includes a total of 3646 hours.

2014 and 2017. . We have excluded the month of April in the R^{1064}_{387} dataset as the mean error between the tropopause and 34 km is $\overline{\sigma_m}(R^{1064}_{387}) = 0.025$. This value is rather high when compared to the other months where $\overline{\sigma_m}(R^{1064}_{387})$ is less than 0.01.

The seasonal cycle for the combined dataset R^{1064} from 208 measurement runs is shown in Fig. 10depicts the aerosol backscatter ratio for R_{1064}. This new dataset, obtained by applying the procedure described in section 3, covers the whole annual cycle in stratospheric aerosol above ALOMAR. The R_{1064} dataset is based on the aforementioned 79 measurement runs with $R_{1064/387}$ plus 129 measurement runs with $R_{1064/355}$ measured in daylight conditions between 2014 and 2017, adding up to a total of 208 measurement runs. Now the dataset also covers the summer months. In the months where both datasets R^{1064} and R^{1064}_{387} are available the datasets agree.

For 2014 to 2017, the R_{1064} and the $R_{1064/387}$ datasets show strong occasional aerosol loads The uncertainties of the monthly mean backscatter ratios R^{1064} result to $\sigma_m(R^{1064}) = 0.06$ at 11 km and $\sigma_m(R^{1064}) = 0.02$ at 34 km and are dominated by the uncertainty of the fit $\tilde{R}^{355}_{387}(z)$.

The R^{1064} and the R^{1064}_{387} datasets both show enhanced aerosol backscatter in September in the lower stratosphere between 12 km and 18 km. These high aerosol levels originate in Canadian wildfires and therefore from wildfires with strong pyrocumulonimbus activity over western Canada . in September 2017. The smoke reached Europe 10 days after its injection in into the lower stratosphere(see Ansmann et al. (2018) for further details) and was detected by the lidar. . This event has been studied in detail by Ansmann et al. (2018) .

During the winter months , (November to March) the peak and the top of the aerosol layer is located at significantly lower altitudes, compared to the rest of the year. In this time period the peak of the layer is found mostly in between 12 to most often found below 22 km. Stratospheric air is sinking This is likely caused by the descending air within the polar vortex in winter.

If However, the location of the ALOMAR observatory is located under close to the edge of the polar vortex, this effect is seen in the aerosol data. Both datasets cover this behaviour wellso during the winter months we observe sometimes air within the vortex and sometimes outside the polar vortex. This results in a variation of the altitudes of the peak of the layer during the winter months.

We have detected A key finding of the new dataset R^{1064} is that the stratospheric aerosol reaches well above 30 kmespecially during summer. We find backscatter ratio values in R_{1064} above . In summer the typical backscatter ratio at 30 km of about 1.05 with a typical uncertainty of 0.02. A presence of aerosol in these altitude ranges is clearly given and should be taken into account in future studies for determining the normalization altitudewhen calculating R.

The ALOMAR RMR lidar is suited to perform stratospheric aerosol measurements throughout the day and the year in the northern polar region. With the lidar, we continuously determine aerosol backscatter ratios (R_{1064}) between the tropopause and 34 . The accuracy of these backscatter profiles is dominated by the random error of the backscatter signal. We calculate the highest uncertainties for very short lidar measurement runs (measurement time under one hour). In these rare cases the uncertainty for the stratospheric aerosol backscatter ratio varies from 0.1 at 10 is $R^{1064} \sim 1.05 \pm 0.02$. So there is clear evidence for aerosols at this altitude. This finding is in contrast to previous studies where the authors assumed an aerosol free altitude starting at 30 km to 0.8 at 34 (McCormick et al., 1984; Barnes and Hofmann, 1997; Khaykin et al., 2017; Zuev et al., 2017) . However, all of the previous studies were performed at mid to low latitudes.

5 Summary and conclusions

We have described the calculation of backscatter ratios using elastic (Rayleigh+Mie) and inelastic (Raman) scattering. For investigation of the stratospheric aerosol layer inelastic scattering is available only during nighttime. To our knowledge no lidar instrument exists that measures the stratospheric aerosol during daytime using the classical Raman method of calculating a backscatter ratio from elastic and inelastic scattering.

An extension of the backscatter ratio time series to daytime using close in time nighttime inelastic signals allows to observe small scale structures present in the stratospheric aerosol even during daytime. We present for the first time multiple sharp background aerosol layers of less than 1 km . Most lidar measurements are longer. For a vertical thickness that partly move in parallel to each other over several days.

To calculate the backscatter ratios R^{1064} and R^{532} during daytime where Raman signals are not available we have developed a proxy that is based on the measured color ratio of elastic scattering at the wavelengths 1064, 532, 355 nm and an empirical correction function. The color ratios with respect to $\lambda = 355$ nm already yield reasonable values for the backscatter ratios. However, the color ratios are about 5 measurement the uncertainty does not exceed 0.02 over the complete altitude range. % smaller than the backscatter ratios.

The challenge of calculating backscatter profiles above ALOMAR during summer was solved by correcting a color ratio available during daylight measurements with a long time mean $\tilde{R}_{355}(z)$ profile fit. The uncertainties of the resulting profiles

~~are dominated by the uncertainty of the correction and result to 0.06 at 11 and 0.02 at 34 for a monthly average of R_{1064}. The difference between $R_{1064/355}$~~ A correction function was calculated from multiple measurements of the backscatter ratio R^{355}_{387} in the period from 2000 to 2018. The measurements show a linear decrease of R^{355}_{387} with altitude. The largest uncertainties on the monthly mean approximated backscatter ratio (R^{1064} and ~~$R_{1064/387}$ gets smaller with~~ R^{532}) are found in the lowest altitudes of the ~~altitude approaching the normalization range of 34 , hence, so does the uncertainty of the R_{1064} backscatter profile. As the R_{1064} dataset is built by the available $R_{1064/387}$ data plus corrected $R_{1064/355}$ data it differs little from $R_{1064/387}$ between September and March. Significant differences occur between April and August due to the addition of large data time (see Fig. 8). The used correction of the aerosol backscatter data will lead to an underestimation of the aerosol in cases of strong aerosol loads. This is due to the fact, that~~ stratospheric aerosol layer, but even there we have observed that the approximated backscatter ratio deviates from the ~~correction fit profile $\tilde{R}_{355}(z)$ was derived from background profiles with common aerosol loads (see Fig. 5). Depending on altitude, the correction has a total effect on the backscatter ratio from 6~~ true backscatter ratio by less than 1% ~~at 10 to no effect at 34~~ .

Using ~~the described methodology, it is possible to investigate the stratospheric aerosol layer above ALOMAR in various ways. For example a single lidar measurement shows strong variations in aerosol backscatter ratio on a 5 minute time resolution (See Fig. 3). Another example is the first year-round~~ this correction function we calculated for the first time a seasonal cycle of backscatter ratios at high latitudes including the summer months. A dedicated seasonal cycle of the ~~stratospheric aerosol measured by lidar in the Arctic. The new dataset also allows the investigation up to decadal scales. Exemplarily, a comparison of monthly mean backscatter ratio from 2014 to 2017 for the nighttime dataset $R_{1064/387}$ (Fig. 9) and the new year-round dataset R_{1064} (Fig. 10) was carried out. The extension of the dataset fills the aerosol backscatter ratio data gap during summer and leads to a year-round dataset~~peak of the aerosol layer with higher altitudes in summer and lower altitudes in winter is found. The top altitude of the layer varies in a similar way throughout the year. The aerosol reaches as high as 34 km during the summer months.

~~Between 2000 and 2018 lidar measurements at ALOMAR where performed on a regular bases. In this timespan we gain 2883 of usable data time for the $R_{1064/387}$ dataset. For the same time this data time raises to 7273 for the R_{1064} dataset.~~

~~In future work, also aerosol backscatter coefficients and extinction coefficients will be derived from the dataset~~We propose to use this new method of calculating the backscatter ratio of the stratospheric aerosol layer from pure elastic scattering for the study of decadal scale variations at high latitudes. Furthermore, the study of variations in stratospheric aerosol at the smallest scales detectable ($dt < 5$ minutes, $dz < 150$ m) will benefit from the method as elastic scattering provides a better signal to noise ratio during night- and daytime.

Code and data availability. The datasets used in this study can be obtained by contacting the first author

Competing interests. The authors declare that they have no conflict of interest.

Acknowledgements. This work benefited from the excellent support of J. Hildebrand, M. Gerding and the dedicated staff at the ALOMAR observatory. The European Centre for Medium-Range Weather Forecasts (ECMWF) is gratefully acknowledged for providing the data. This project is supported by DFG (Deutsche Forschungsgesellschaft, Projektnummer 312991878)

References

SPARC Assessment of Stratospheric Aerosol Properties (ASAP), Tech. rep., SPARC, http://www.sparc-climate.org/publications/sparc-reports/, 2006.

Andersson, S. M., Martinsson, B. G., Vernier, J.-P., Friberg, J., Brenninkmeijer, C. ~~A.~~A. M., Hermann, M., ~~Van Velthoven~~van Velthoven, P. ~~F.~~F. J., and Zahn, A.: Significant radiative impact of volcanic aerosol in the lowermost stratosphere, Nature ~~communications~~Communications, 6, 7692, doi:10.1038/ncomms8692, 2015.

Ansmann, A., Riebesell, M., and Weitkamp, C.: Measurement of atmospheric aerosol extinction profiles with a Raman lidar, Optics Letters, 15, 746–748, doi:10.1364/ol.15.000746, 1990.

Ansmann, A., Baars, H., Chudnovsky, A., Mattis, I., Veselovskii, I., Haarig, M., Seifert, P., Engelmann, R., and Wandinger, U.: Extreme levels of Canadian wildfire smoke in the stratosphere over central Europe on ~~21–22 August~~21–22 August 2017, Atmospheric Chemistry and Physics, 18, 11 831–11 845, doi:10.5194/acp-18-11831-2018, 2018.

Barnes, J. E. and Hofmann, D. J.: Lidar measurements of stratospheric aerosol over Mauna Loa Observatory, Geophysical Research Letters, 24, 1923–1926, doi:10.1029/97gl01943, 1997.

Bartusek, K. and Gambling, D.: Simultaneous measurements of stratospheric aerosols using lidar and the twilight technique, Journal of Atmospheric and Terrestrial Physics, 33, 1415–1430, doi:10.1016/0021-9169(71)90013-4, http://www.sciencedirect.com/science/article/pii/0021916971900134, 1971.

Baumgarten, G.: Doppler Rayleigh/Mie/Raman lidar for wind and temperature measurements in the middle atmosphere up to 80 km, Atmospheric Measurement Techniques, 3, 1509–1518, doi:10.5194/amt-3-1509-2010, 2010.

Baumgarten, G., Lübken, F.-J., and Fricke, K. H.: First observation of one noctilucent cloud by a twin lidar in two different directions, ~~Ann. Geophys.~~Annales Geophysicae, 20, 1863–1868, doi:10.5194/angeo-20-1863-2002, 2002.

Baumgarten, G., Fiedler, J., Lübken, F.-J., and ~~von Cossart~~von Cossart, G.: Particle properties and water content of noctilucent clouds and their interannual variation, ~~J. Geophys. Res.~~Journal of Geophysical Research, 113, D06203, doi:10.1029/2007jd008884, 2008.

~~Brion, J., Chakir, A., Charbonnier, J., Daumont, D., Parisse, C. , and Malicet, J~~

Beyerle, G. and Neuber, R.: ~~Absorption spectra measurements for the ozone molecule in the 350–830 nm region~~The stratospheric aerosol content above Spitzbergen during winter 1991/92, ~~Journal of atmospheric chemistry, 30, 291–299, 1998.~~ Geophysical Research Letters, 21, 1291–1294, doi:10.1029/93gl03292, 1994.

Deshler, T., Anderson-Sprecher, R., Jäger, H., Barnes, J., Hofmann, D. J., Clemesha, B., Simonich, D., Osborn, M., Grainger, R. G., and Godin-Beekmann, S.: Trends in the nonvolcanic component of stratospheric aerosol over the period ~~1971–2004~~1971–2004, Journal of Geophysical Research~~: Atmospheres~~, 111, doi:10.1029/2005jd006089, 2006.

English, J. M., Toon, O. B., Mills, M. J., and Yu, F.: Microphysical simulations of new particle formation in the upper troposphere and lower stratosphere, ~~Atmos. Chem. Phys~~Atmospheric Chemistry and Physics, 11, 9303–9322, doi:10.5194/acp-11-9303-2011, 2011.

Fernald, F. G.: Analysis of atmospheric lidar observations: some comments, ~~Appl. Opt.~~Applied Optics, 23, 652–653, doi:10.1364/ao.23.000652, 1984.

Fiedler, J., Baumgarten, G., and von Cossart, G.: A middle atmosphere lidar for multi-parameter measurements at a remote site, 24th ILRC, pp. 824–827, 2008.

Fyfe, J.~~,~~ C., von Salzen, K.~~ v.~~, Cole, J. N. S., Gillett, N. P., and Vernier, J.-P.: Surface response to stratospheric aerosol changes in a coupled ~~atmosphere–ocean~~ atmosphere-ocean model, Geophysical Research Letters, 40, 584–588, doi:10.1002/grl.50156, 2013.

Gerding, M., Baumgarten, G., Blum, U., Thayer, J. P., Fricke, K.-H., Neuber, R., and Fiedler, J.: Observation of an unusual mid-stratospheric aerosol layer in the Arctic: possible sources and implications for polar vortex dynamics, Annales Geophysicae, 21, 1057–1069, doi:10.5194/angeo-21-1057-2003, 2003.

Gorshelev, V., Serdyuchenko, A., Weber, M., Chehade, W., and Burrows, J. P.: High spectral resolution ozone absorption ~~cross-sections–Part~~ cross-sections-Part 1: Measurements, data analysis and comparison with previous measurements around 293 K, Atmospheric Measurement Techniques, 7, 609–624, doi:10.5194/amt-7-609-2014, 2014.

~~Hofmann, D., Rosen, J., and Gringel, W.: Delayed production of sulfuric acid condensation nuclei in the polar stratosphere from El Chichon volcanic vapors, Journal of Geophysical Research: Atmospheres, 90, 2341–2354, 1985.~~

Hofmann, D., Barnes, J., O~~'~~'Neill, M., Trudeau, M., and Neely, R.: Increase in background stratospheric aerosol observed with lidar at Mauna Loa Observatory and Boulder, Colorado, Geophysical Research Letters, 36, n/a–n/a, doi:10.1029/2009gl039008, 2009.

~~Judd, J. W., Strachey, R., Wharton, W. J. L., Evans, F. J., Russell, F. A. R., Archibald, D~~

Hofmann, D. J., Rosen, J. M., and ~~Whipple, G. M~~Gringel, W.: ~~The Eruption of Krakatoa: And Subsequent Phenomena~~Delayed production of sulfuric acid condensation nuclei in the polar stratosphere from El Chichon volcanic vapors, ~~Trbner Company, 1888.~~ Journal of Geophysical Research, 90, 2341, doi:10.1029/jd090id01p02341, 1985.

Junge, C. E. and Manson, J. E.: Stratospheric aerosol studies, Journal of Geophysical Research, 66, 2163–2182, doi:10.1029/jz066i007p02163, 1961.

Junge, C. E., Chagnon, C. W., and Manson, J. E.: ~~Stratospheric aerosols~~STRATOSPHERIC AEROSOLS, Journal of Meteorology, 18, 81–108, doi:10.1175/1520-0469(1961)018<0081:sa>2.0.co;2, 1961a.

Junge, C. E., Chagnon, C. W., and Manson, J. E.: A World-wide Stratospheric Aerosol Layer, Science, 133, 1478–1479, doi:10.1126/science.133.3463.1478-a, http://science.sciencemag.org/content/133/3463/1478.2, 1961b.

Khaykin, S. M., Godin-Beekmann, S., Keckhut, P., Hauchecorne, A., Jumelet, J., Vernier, J.-P., Bourassa, A., Degenstein, D. A., Rieger, L. A., Bingen, C., ~~et al~~Vanhellemont, F., Robert, C., DeLand, M., and Bhartia, P. K.: Variability and evolution of the midlatitude stratospheric aerosol budget from 22 years of ground-based lidar and satellite observations, Atmospheric Chemistry and Physics, 17, 1829–1845, doi:10.5194/acp-17-1829-2017, 2017.

Klett, J. D.: Lidar inversion with variable backscatter/extinction ratios, ~~Appl. Opt.~~Applied Optics, 24, ~~1638–1643,~~ 1638, doi:10.1364/ao.24.001638, http://ao.osa.org/abstract.cfm?URI=ao-24-11-1638, 1985.

Kovalev, V. A. and Eichinger, W. E.: Elastic Lidar, John Wiley & Sons, Inc., doi:10.1002/0471643173, 2004.

Kremser, S., Thomason, L. W., von Hobe, M., Hermann, M., Deshler, T., Timmreck, C., Toohey, M., Stenke, A., Schwarz, J. P., Weigel, R., Fueglistaler, S., Prata, F. J., Vernier, J.-P., Schlager, H., Barnes, J. E., Antuña-Marrero, J.-C., Fairlie, D., Palm, M., Mahieu, E., Notholt, J., Rex, M., Bingen, C., Vanhellemont, F., Bourassa, A., Plane, J. M. C., Klocke, D., Carn, S. A., Clarisse, L., Trickl, T., Neely, R., James, A. D., Rieger, L., Wilson, J. C., and Meland, B.~~, and Antuna-Marrero, J.-C.~~: Stratospheric ~~aerosol—Observations~~aerosol-Observations, processes, and impact on climate, Reviews of Geophysics, 54, 278–335, doi:10.1002/2015rg000511, https://agupubs.onlinelibrary.wiley.com/doi/abs/10.1002/2015RG000511, 2016.

McCormick, M., Swissler, T., Fuller, W., Hunt, W., and Osborn, M.: Airborne and ground-based lidar measurements of the El Chichon stratospheric aerosol from 90 N to 56 S, Geofisica Internacional, 23, 1984.

McCormick, M. P., Thomason, L. W., and Trepte, C. R.: Atmospheric effects of the Mt Pinatubo eruption, Nature, 373, ~~399~~399–404, doi:10.1038/373399a0, 1995.

Penndorf, R.: Tables of the ~~refractive index for standard air~~ Refractive Index for Standard Air and the Rayleigh ~~scattering coefficient for the spectral region between 0.2 and 20.0~~ Scattering Coefficient for the Spectral Region between 02 and 200 μ and ~~their application to atmospheric optics~~Their Application to Atmospheric Optics, ~~Josa~~Journal of the Optical Society of America, 47, ~~176–182~~176, doi:10.1364/josa.47.000176, 1957.

Peter, T.: ~~Microphysics and heterogeneous chemistry of polar stratospheric clouds~~MICROPHYSICS AND HETEROGENEOUS CHEMISTRY OF POLAR STRATOSPHERIC CLOUDS, Annual Review of Physical Chemistry, 48, 785–822, doi:10.1146/annurev.physchem.48.1.785, 1997.

~~Raman, C. V.: A new radiation, 1928.~~

~~Rayleigh, L.: On the scattering of light by small particles, The London, Edinburgh, and Dublin Philosophical Magazine and Journal of Science, 41~~

Picone, J. M., ~~447–454~~Hedin, A. E., ~~1871.~~

~~Rayleigh, L~~Drob, D. P., and Aikin, A. C.: ~~XXXIV. On the transmission of light through an atmospherecontaining small particles in suspension, and on the origin of the blue of the sky~~NRLMSISE-00 empirical model of the atmosphere: Statistical comparisons and scientific issues, ~~The London, Edinburgh, and Dublin Philosophical Magazine and Journal of Science, 47, 375–384, 1899.~~ Journal of Geophysical Research: Space Physics, 107, SIA 15–1–SIA 15–16, doi:10.1029/2002ja009430, 2002.

Robock, A. and Mao, J.: The ~~volcanic signal in surface temperature observations~~Volcanic Signal in Surface Temperature Observations, Journal of Climate, 8, 1086–1103, doi:10.1175/1520-0442(1995)008<1086:tvsist>2.0.co;2, 1995.

Rosenlof, K., Hassler, B., Bodeker, G., and NOAA CDR Program: NOAA Climate Data Record (CDR) of Zonal Mean Ozone Binary Database of Profiles (BDBP), version 1.0, doi:10.7289/v56m34rt, 2015.

Santer, B. D., Bonfils, C., Painter, J. F., Zelinka, M. D., Mears, C., Solomon, S., Schmidt, G. A., Fyfe, J. C., Cole, J. ~~N.~~N. S., Nazarenko, L., ~~et al~~Taylor, K. E., and Wentz, F. J.: Volcanic contribution to decadal changes in tropospheric temperature, Nature Geoscience, 7, ~~185~~185–189, doi:10.1038/ngeo2098, 2014.

Santer, B. D., Solomon, S., Bonfils, C., Zelinka, M. D., Painter, J. F., Beltran, F., Fyfe, J. C., Johannesson, G., Mears, C., Ridley, D. A., ~~et al~~Vernier, J.-P., and Wentz, F. J.: Observed multivariable signals of late 20th and early 21st century volcanic activity, Geophysical Research Letters, 42, 500–509, doi:10.1002/2014gl062366, 2015.

Solomon, S., Daniel, J. S., Neely, R. R., Vernier, J.-P., Dutton, E. G., and Thomason, L. W.: The Persistently Variable ~~"Background"~~"Background" Stratospheric Aerosol Layer and Global Climate Change, Science, 333, 866–870, doi:10.1126/science.1206027, http://science.sciencemag.org/content/333/6044/866, 2011.

~~Thomason, L. and Peter, T~~

Symons, G.: ~~Assessment of stratospheric aerosol properties (ASAP)~~The eruption of Krakatoa, and subsequent phenomena : report of the Krakatoa committee of the Royal Society, ~~Available online: www. sparc-climate. org/publications/sparc-reports/(accessed on 1 December 2015), 2006.~~ printed by Harrison and Sons, doi:10.3931/e-rara-16337, 1888.

Trickl, T., Giehl, H., Jäger, H., and Vogelmann, H.: 35 yr of stratospheric aerosol measurements at Garmisch-Partenkirchen: from Fuego to Eyjafjallajökull, and beyond, Atmospheric Chemistry and Physics, 13, 5205–5225, doi:10.5194/acp-13-5205-2013, 2013.

Vernier, J.-P., Thomason, L. W., Pommereau, J.-P., Bourassa, A., Pelon, J., Garnier, A., Hauchecorne, A., Blanot, L., Trepte, C., Degenstein, D., ~~et al~~and Vargas, F.: Major influence of tropical volcanic eruptions on the stratospheric aerosol layer during the last decade, Geophysical Research Letters, 38, n/a–n/a, doi:10.1029/2011gl047563, 2011.

Vernier, J.-P., Fairlie, T. D., Natarajan, M., Wienhold, F. G., Bian, J., Martinsson, B. G., Crumeyrolle, S., Thomason, L. W., and Bedka, K. M.: Increase in upper tropospheric and lower stratospheric aerosol levels and its potential connection with Asian pollution, Journal of Geophysical Research: Atmospheres, 120, 1608–1619, doi:10.1002/2014jd022372, 2015.

~~von Cossart~~

von Cossart, G., Fiedler, J., and ~~von Zahn~~von Zahn, U.: Size ~~distribution~~ distributions of NLC particles as determined from ~~3-color~~ 3-color observations of NLC by ground-based ~~Lidar~~lidar, ~~Geophys. Res. Lett.~~Geophysical Research Letters, 26~~(11)~~, 1513–1516, doi:10.1029/1999gl900226, 1999.

~~von Savigny~~

von Savigny, C., Ernst, F., Rozanov, A., Hommel, R., Eichmann, K.-U., Rozanov, V., Burrows, J. P., and Thomason, L. W.: Improved stratospheric aerosol extinction profiles from ~~SCIAMACHY~~SCIAMACHY: validation and sample results, Atmospheric Measurement Techniques Discussions, 8, ~~5223–5235~~8353–8383, doi:10.5194/amtd-8-8353-2015, 2015.

von Zahn, U., von Cossart, G., Fiedler, J., Fricke, K. H., Nelke, G., Baumgarten, G., Rees, D., Hauchecorne, A., and Adolfsen, K.: The ~~ALOMAR~~ ALOMAR Rayleigh/Mie/Raman lidar: objectives, configuration, and performance, Annales Geophysicae, 18, 815–833, doi:10.1007/s00585-000-0815-2, https://doi.org/10.1007/s00585-000-0815-2, 2000.

Yu, P., Toon, O. B., Neely, R. R., Martinsson, B. G., and Brenninkmeijer, C. ~~A.~~A. M.: Composition and physical properties of the Asian ~~tropopause aerosol layer~~ Tropopause Aerosol Layer and the North American ~~tropospheric aerosol layer~~Tropospheric Aerosol Layer, Geophysical ~~research letters~~Research Letters, 42, 2540–2546, doi:10.1002/2015gl063181, 2015.

~~Simplified overview of the polychromatic detection system of the ALOMAR RMR lidar. The light collected by the telescopes enters the optical bench on the middle left side of the sketch. It is then separated by wavelength via dichroic mirrors (D) and intensity via beam splitters (BS). In daylight conditions, the light is guided through etalons to suppress solar background. At the end of each branch, the photons are converted to electrical pulses using avalanche photo diodes and photomultiplier tubes and then counted by the detection electronics. The identification mark for these detectors is built as follows: first letter: spectral range (U-ultraviolet, V-visible, I-infrared), last letter: sensitivity (L-low, M-middle, H-high). Further letters "VR" for vibrational Raman,~~

~~Averaged altitude profiles of backscattered signals for different counters of the RMR lidar for a 17 long measurement in January 2018. The upper panels show the original count rate, the lower ones the resulting profiles after combining the signals of the different altitude ranges. On the left side for nighttime data and on the right side for daytime data. The altitude range of the stratospheric aerosol layer is shown in gray. The increase in the profiles below 30 is caused by tropospheric and polar stratospheric clouds. The plots show an average of both laser/telescope systems of the lidar.~~

~~Stratospheric aerosol backscatter ratio ($R_{1064/387}$) for a measurement starting 17:30 on February 18th 2018. The time resolution is 5 minutes and the altitude resolution is 150 . Black bars at the top indicate nighttime configuration. At the bottom end, data is cut at the tropopause.~~

~~Backscatter ratio and color ratio profiles for a 97 measurement starting 07:45 on October 10th 2015. 46 of the data have been measured in daytime configuration and 51 in nighttime configuration. The green ($R_{1064/387}$) and the cyan ($R_{532/387}$) curves show the backscatter ratio which is not available in summer. The red ($CR_{1064/355}$) and the yellow ($CR_{532/355}$) curves show a color ratio, where aerosol signal is present in both counters. The blue curve shows a $R_{355/387}$ backscatter ratio which is used to correct the $CR_{1064/355}$ and $CR_{532/355}$ color ratios. The grey area at the top indicates part of the normalization altitude. Coloured shaded areas around the lines indicate the measurement uncertainty. The grey line at 13 indicates the tropopause.~~

$R_{355/387}$ profiles from 2000 to 2018 (grey). Each line is a nighttime measurement run average. The total nighttime measurement time of all profiles is 1789 . Profiles are filtered for runs without PSC. The linear fit of the mean profile is drawn in blue ($\tilde{R}_{355}(z)$) with the uncertainty being the standard deviation of the $R_{355/387}$ profiles.

Backscatter ratio and color ratio profiles for a 97 measurement starting 07:45 on October 10th 2015. 46 of the data have been measured in daytime configuration and 51 in nighttime configuration. The green ($R_{1064/387}$) and the cyan ($R_{532/387}$) curves show the backscatter ratio which is not available in summer. The red ($CR_{1064/355}$) and the yellow ($CR_{532/355}$) curves show a color ratio, where aerosol signal is present in both counters. The blue curve shows the $\tilde{R}_{355}(z)$ average backscatter ratio which is used to correct the $CR_{1064/355}$ and $CR_{532/355}$ color ratios, using equation 13. The grey area at the top indicates part of the normalization altitude. Coloured shaded areas around the lines indicate the measurement uncertainty. The grey line at 13 indicates the tropopause. This results in the corrected color ratios $R_{1064/355}$ (purple) and $R_{532/355}$ (orange) for this measurement.

Altitude profiles of the difference of $R_{1064/387}$ and $R_{1064/355}$ for each measurement between 2000 and 2018 where both ratios are available (red lines, 103 profiles). The red shadowed area shows the standard deviation of the profiles. The black line depicts the mean difference.

Time of available data for each month in the years 2014 to 2017 for $R_{1064/387}$ (blue) and R_{1064} (orange).

Mean seasonal cycle of aerosol backscatter ratio $R_{1064/387}$ over the time span 2014 to 2017. The backscatter ratio was calculated from hourly averaged lidar data and averaged per month afterwards. The seasonal cycle is calculated from 79 measurement runs with a total of 1255 .

Mean seasonal cycle of aerosol backscatter ratio R_{1064} over the time span 2014 to 2017. The backscatter ratio was calculated from hourly averaged lidar data and averaged per month afterwards. The seasonal cycle is calculated from 208 measurement runs with a total of 3646 .

Zuev, V. V., Burlakov, V. D., Nevzorov, A. V., Pravdin, V. L., Savelieva, E. S., and Gerasimov, V. V.: 30-year lidar observations of the stratospheric aerosol layer state over Tomsk (Western Siberia, Russia), Atmospheric Chemistry and Physics, 17, 3067–3081, doi:10.5194/acp-17-3067-2017, 2017.